FoxA1 and FoxA2 regulate growth and cellular identity in NKX2-1-positive lung adenocarcinoma

Grace Orstad[1,2], Alex Jones[1,3,5], Brian Lohman[1,4], Katherine L. Gillis[1,2], Eric L. Snyder[1,2,3]

Affiliations

1. Huntsman Cancer Institute, University of Utah, Salt Lake City, Utah, USA
2. Department of Oncological Sciences, University of Utah, Salt Lake City, Utah, USA
3. Department of Pathology, University of Utah, Salt Lake City, Utah, USA
4. Bioinformatics Shared Resource, Huntsman Cancer Institute, University of Utah, Salt Lake City, Utah, USA
5. Current affiliation: HCI Clinical Trials Operations, Huntsman Cancer Institute, University of Utah, Salt Lake City, Utah, USA

Corresponding author: eric.snyder@hci.utah.edu

Key words: FoxA1, FoxA2, NKX2-1, lung adenocarcinoma, cellular identity

ABSTRACT

Change in cancer cell identity is well characterized as a mechanism of cancer progression and acquired resistance to targeted therapies. Lung adenocarcinoma (LUAD) exhibits significant heterogeneity in cell identity and differentiation state; these characteristics correlate directly with prognosis, response to available therapies, and acquisition of drug resistance. In previous work, we have shown that FoxA1 and FoxA2 (FoxA1/2) activate a gastric differentiation program in NKX2-1-negative LUAD. Here we investigate the role of FoxA1/2 in NKX2-1-positive LUAD. We find that FoxA1/2 are consistently expressed in NKX2-1-positive human LUAD. *Foxa1/2* deletion severely impairs proliferation and significantly prolongs overall survival in a genetically engineered mouse model of KRAS-driven LUAD. FoxA1/2 activate expression of a mixed-lineage transcriptional program characterized by co-expression of pulmonary (Alveolar Type II) and gastrointestinal marker genes. Loss of FoxA1/2 causes a lineage switch, activating gene expression programs associated with Alveolar Type I cells and maturing squamous epithelial cells. Inhibition of NKX2-1 partially rescues the antiproliferative impact of FoxA1/2 loss, showing that NKX2-1 retains some degree of activity in FoxA1/2-null cells, despite its inability to activate canonical target genes. In summary, this study identifies FoxA1/2 expression as a novel vulnerability in NKX2-1 positive LUAD and shows that FoxA1/2 actively regulate cellular identity in this disease.

INTRODUCTION

The behavior of a cancer cell is initially constrained by the specific epigenetic state of its cell of origin. Changes in cancer cell identity (often referred to as lineage switching, lineage plasticity, or histological transformation) have become increasingly well characterized as a mechanism of cancer progression and acquired resistance to targeted therapies[1-3]. Lung cancer is the leading cause of cancer death worldwide, and lung adenocarcinoma (LUAD) is the most frequently diagnosed subtype of this disease[4]. In patients, LUAD exhibits significant heterogeneity in cell identity and differentiation state[5]; these characteristics correlate directly with prognosis, response to available therapies, and acquisition of drug resistance[6-9]. Despite these correlations, the field lacks a comprehensive understanding of what governs LUAD cell identity and how perturbations within these networks alter malignant potential.

Previous work from our lab and others has shown that the transcription factors FoxA1, FoxA2, and NKX2-1/TTF1 coordinately regulate cellular identity in LUAD[10-14]. The homeodomain transcription factor NKX2-1/TTF1 is a master regulator of normal lung morphogenesis and differentiation[15-18] as well as LUAD identity[12-14]. NKX2-1 activity is dependent on differential interactions with many transcriptional co-activators and co-repressors in a gene-specific manner, including FoxA1 and FoxA2 (FoxA1/2) in both normal and malignant lung tissue[17,19-25]. FoxA1/2 physically interact with NKX2-1, which enhances the expression of NKX2-1 target genes that have both NKX2-1 and FoxA binding sequences in the promoter[26]. FoxA1 and FoxA2 are closely related members of the forkhead box transcription factor family[27]. They are highly homologous and share many cellular roles including establishing and maintaining cellular identity in multiple endodermal-derived tissues[28]. FoxA1/2 are critical regulators of normal foregut differentiation; embryonic deletion in the foregut endoderm blocks hepatic specification[29,30], pancreatogenesis[31], and branching morphogenesis of the lung[32]. FoxA2 is activated at E6.5 in endoderm precursor tissue, followed by FoxA1 at E8.5[33]. They are co-expressed as NKX2-1 is activated at E9.5[33,34] to specify the development of the prospective lung domain of the gut tube, and continue to be expressed in the lung throughout organogenesis. In the adult mouse lung, FoxA1/2 are expressed specifically within the trachea, bronchiolar epithelium, and Type II Alveolar cells[35,36].

FoxA1 and FoxA2 play context-specific roles in multiple types of cancer[37]. For example, FoxA1 functions as an oncogene in breast and prostate cancer by virtue of genomic amplifications and point mutations within the forkhead box DNA binding domain activity[38-40]. In LUAD, we have previously shown that NKX2-1 regulates FoxA1/2 function and genomic binding[12]. In NKX2-1-negative LUAD, FoxA1/2 drive a gastric differentiation program, likely reflecting their role in normal foregut differentiation. These NKX2-1-negative tumors closely resemble a subtype of the human disease called invasive mucinous adenocarcinoma (IMA), which also exhibits gastric differentiation[41]. When NKX2-1 is expressed, it recruits FoxA1/2 to regulatory elements of pulmonary marker genes, resulting in extensive genomic co-localization between these transcription factors in both human[13,42] and murine[12] NKX2-1-positive LUAD. This suggests FoxA1/2 and NKX2-1 may have cooperative functions in LUAD that mirror their functions in normal tissue. Further supporting this possibility, ~10% of human LUAD exhibit co-amplification of the genomic region containing both *NKX2-1* and *FOXA1*. In a functional screen of nuclear receptors and their co-regulators in human LUAD cell lines, FOXA1 was identified as pro-tumorigenic

in a subset of the cell lines analyzed: those with higher *FOXA1* copy number or higher FOXA1 expression exhibit varied levels of dependency on the gene, while cell lines with low levels of FOXA1 do not[43].

Despite these observations, FoxA1 and FoxA2 have not been systematically characterized via *in vivo* models of NKX2-1-positive LUAD, which comprises ~75% of human LUAD cases overall[44]. Here we use GEMMs to show that FoxA1/2 are critical regulators of growth and cellular identity in KRAS-driven NKX2-1-positive LUAD.

RESULTS AND DISCUSSION

FoxA1/2 are required for growth of NKX2-1-positive lung adenocarcinoma

In order to understand the role of FoxA1/2 in LUAD we first evaluated whole sections and tumor microarrays from a total of 132 human LUAD tissue samples. Histological analysis of these human tumors showed that all NKX2-1 positive tumors evaluated (n=87) express FoxA1 and/or FoxA2. In contrast, 17% (8/45) of NKX2-1-negative tumors have no detectable FoxA1 or FoxA2 expression (Supplemental Figure 1A-B, $p<0.0001$, Fisher's Exact test). These initial observations show that NKX2-1 and FoxA1/2 are frequently co-expressed in human LUAD. NKX2-1 and FoxA1/2 are also co-expressed (Figure 1A, left panels) in the LUAD GEMM driven by $KRAS^{G12D}$ and deletion of *Trp53* ("KP" hereafter). This data suggests that there is selective pressure for NKX2-1 positive LUAD tumors to retain FoxA1/2, and that NKX2-1-positive disease is dependent on FoxA1/2 activity. Consistent with this possibility, we have previously shown that stochastic NKX2-1 loss precedes FoxA2 loss in the KP model[11].

To test this directly, we developed a sequential recombination system that enables us to delete *Foxa1* and/or *Foxa2* in existing KRAS driven, NKX2-1 positive lung tumors *in vivo*. We generated mice harboring the following FlpO-recombinase targeted alleles: heterozygous activation of oncogenic $Kras^{G12D}$ ($Kras^{FSF\text{-}G12D/+}$)[45], homozygous inactivation of tumor suppressor *Trp53* ($Trp53^{Frt/Frt}$)[46], and homozygous expression of tamoxifen-activated Cre-recombinase ($Rosa^{FSF\text{-}CreERT2}$)[47]. This model also has Cre-recombinase targeted conditional alleles of *Foxa1*[31] and/or *Foxa2*[48]. Upon tamoxifen treatment, Cre^{ERT2} enters the nucleus and deletes *Foxa1* and/or *Foxa2* (KPF_1, KPF_2, or KPF_1F_2 hereafter) specifically in LUAD cells (Supplemental Figure 1C). We first used this model system to determine the effect of *Foxa1/2* deletion at an early timepoint in tumor development. Lung

tumors were initiated by intubation with adenoviral FlpO-recombinase and allowed to develop for 6 weeks before deletion of *Foxa1/2* via tamoxifen treatment. Eight weeks after tumor initiation, lung tissue was collected and evaluated histologically (Figure 1A). Heterozygous deletion of a single copy of *Foxa1* and *Foxa2* ($KPF_1^{F/+}F_2^{F/+}$), as well as homozygous deletion of either *Foxa1* (KPF_1) or *Foxa2* (KPF_2) alone has no effect on tumor proliferation (Figure 1B) or overall tumor burden (Figure 1C). Simultaneous deletion of both *Foxa1* and *Foxa2* causes a significant decrease in both proliferation (7.8 fold decrease) and overall tumor burden at an early timepoint (Figure 1B-C), demonstrating that low-grade LUAD tumors are dependent on FoxA1/2.

In order to delineate the role of FoxA1/2 in late-stage and higher grade adenocarcinomas, we performed a long-term survival study in which tumors developed for 10 weeks prior to tamoxifen or vehicle injections. At this timepoint tumors within the KP mouse model are known to have progressed to higher grade, macroscopic lesions[49]. Complete deletion of both *Foxa1* and *Foxa2* in established tumors leads to a significant increase in survival, increasing median lifespan by 13.5 weeks (Figure 1D). In contrast, deletion of a single copy of both *Foxa1* and *Foxa2* (Figure 1E), or *Foxa2* alone (Supplemental Figure 1 F-G), has no impact on median overall survival. Deletion of *Foxa1* alone (Supplemental Figure 1 D-E) led to a slight (1.5 week) increase in survival. However, *Foxa1* deletion had no obvious impact on relevant tumor phenotypes in this analysis, suggesting that this increase is unlikely to be biologically significant (Supplemental Table 1). Of note, vehicle and tamoxifen-treated KPF_1 mice had a slightly shorter median survival than controls of all other genotypes, suggesting that a locus linked to the *Foxa2* conditional allele (or the allele itself) may modify tumor initiation in this model. Immunohistochemical (IHC) analysis demonstrated high levels of recombination in tamoxifen-treated KPF_1, KPF_2 and KPF_1F_2 mice, although incomplete recombinants could also be detected in most mice (data not shown). Together, these results establish that FoxA1 and FoxA2 are necessary for NKX2-1-positive LUAD tumor development.

We derived cell lines from individual macroscopic KPF_1F_2 tumors under either standard 2D (3311) or three-dimensional, Matrigel-based organoid (1027B, 1027D, and 1292B) culture conditions. Treatment of these cultures with 4-hydroxytamoxifen (4-OHT) generates isogenic pairs in which the only difference is the presence or absence of FoxA1/2 (Figure 2A, Supplemental Figure 2A). In agreement with our *in vivo* data, *in vitro* deletion

of *Foxa1/2* in both cell lines and organoids leads to a significant decrease in proliferation (Figure 2B-C). We subcutaneously injected the 3311 cell line into NOD-SCID-gamma chain deficient (NSG) mice and treated with either vehicle or tamoxifen when tumors reached an average volume of ~200mm^3. Deletion of *Foxa1/2* causes initial tumor regression, followed by slower growth (Figure 2D-E, see also 4H). Histopathologic analysis identified two distinct morphologies in *Foxa1/2*-deleted subcutaneous tumors: a moderate to poorly differentiated carcinoma component (similar to controls) and a distinct sarcomatoid/quasi-mesenchymal component, which exhibited diminished NKX2-1 levels (Figure 2D). Combined, these results demonstrate that FoxA1/2 are required for the growth of NKX2-1 positive LUAD *in vitro* and *in vivo*.

FoxA1/2 regulate multiple cellular identity programs in NKX2-1-positive lung adenocarcinoma

In order to understand the impact of FoxA1/2 loss on the transcriptome of NKX2-1-positive LUAD, we performed RNAseq on isogenic KPF$_1$F$_2$ organoid pairs. We identified 802 differentially expressed genes: 402 in FoxA1/2-positive organoids and 400 in FoxA1/2-positive organoids (Supplemental Figure 3A, Supplemental Table 2). Deletion of *Foxa1/2* in organoid cultures leads to decreased expression of multiple canonical pulmonary marker genes (Figure 3A), many of which are known NKX2-1-target genes. We confirmed downregulation of two proteins encoded by these genes after *Foxa1/2*-deletion in autochthonous tumors (SPB and SPC, Figure 3B and Supplemental Figure 3B). Thus, FoxA1/2 are required for full pulmonary differentiation in KP LUAD, despite the continued expression of NKX2-1 after *Foxa1/2* deletion (Figure 1A, 2A and Supplemental Figure 2A).

Somewhat surprisingly, multiple transcripts associated with gastrointestinal (GI) differentiation were also downregulated after *Foxa1/2* deletion in organoids (Figure 3C), and we also observed a decrease in HNF4α protein levels after *Foxa1/2* deletion *in vivo* (Figure 3D). Although several of these GI marker genes are activated by FoxA1/2 in NKX2-1-negative LUAD, they are typically repressed by NKX2-1 in p53-proficient LUAD, in part by regulation of FoxA1/2 binding[10,12]. However, recent work suggests that p53-null tumors may have increased plasticity compared to p53-proficient tumors and can upregulate elements of GI differentiation despite NKX2-1 expression. Specifically, an extensive scRNA-seq analysis of tumor progression in the KP LUAD GEMM defined 11 distinct transcriptional programs that emerge as tumors progress from small precursor lesions to high grade adenocarcinomas[50]. Early low grade tumor cells most closely resemble normal alveolar type 2 (AT2) cells, as

evidenced by expression of *Nkx2-1* and its canonical AT2 targets. Later on (12-30 weeks after initiation), subsets of higher grade LUAD cells upregulate distinct GI transcriptional programs despite the continued expression of *Nkx2-1*, thus adopting a mixed lineage state. In late stage disease, a sub-population of cells reach a terminal EMT-like, poorly differentiated transcriptional state. Although transition through these states is thought to be a key component of malignant progression, the mechanisms driving these lineage changes have not been fully defined.

To assess the effect of *Foxa1/2* deletion on these transcriptional programs, we used Gene Set Enrichment Analysis (GSEA) to measure their enrichment in our differentially expressed genes (Figure 3G, Supplemental Figure 3C-D). We found that 8 of the 11 transcriptional programs are enriched in FoxA1/2-positive LUAD organoids, including the pulmonary AT2-like program and several GI-related programs (Gastric-like, GI epithelium-like, Hepatic-Gastric/Inflammation). In contrast, three programs are enriched in FoxA1/2-negative organoids: the de-differentiated Alveolar Type I/Alveolar Type II (AT1/AT2), EMT, and stress-response programs. Taken together, these data show that FoxA1/2 are required for both the AT2-like program found in early lesions and also for activation of mixed lineage (pulmonary+GI) states adopted by a subset of tumor cells during cancer progression.

Global pathway analysis (GSEA) provided additional insights into the cellular identities adopted by FoxA1/2-null cells. We find consistent enrichment of gene sets canonically found in maturing stratified squamous epithelium in FoxA1/2-negative organoids across multiple MSigDB collections. Gene sets associated with keratinocyte differentiation, as well as the cornified envelope, and more broad categorizations of squamous tumors and epidermal cell differentiation are all enriched in FoxA1/2-negative organoids (Figure 3 E&H, Supplemental Table 3). The stratified squamous epithelium, which is found in the esophagus, oropharyngeal mucosa, and epidermis, has distinct layers with unique cellular identities. Basal cells are ΔNp63-positive and contain a pool of stem cells that then commit to terminally differentiate and migrate away from the basement membrane toward the epithelial surface. As cells mature, they differentiate and lose expression of ΔNp63, forming additional layers (e.g. spinous cell and granule cell) with distinct gene expression programs that ultimately become fully keratinized in some anatomic locations (reviewed in Zou et al[51]). To define the cell type(s) that FoxA1/2-null organoids most closely

resemble, we intersected our data with the transcriptional identities of unique epidermal cell populations, which were recently characterized by scRNA-seq human skin[51]. Zou et al classified epidermal cells into the following subcategories based on unique transcriptional profiles: undifferentiated epidermal cells encompassing basal cell and proliferating mitotic cell subpopulations, and differentiated keratinocytes encompassing spinous cells and terminally differentiated granular cells. The spinous cell program was the most significantly enriched of all epidermal cell types in FoxA1/2 null organoids (False Discovery Rate 0.000; Normalized Enrichment Score -1.91). The granular cell program was also significantly enriched in FoxA1/2 null organoids (False Discovery Rate 0.000; Normalized Enrichment Score -1.67), but the transcriptional programs of the undifferentiated epidermal cell populations were not. As predicted by this analysis, the master transcriptional regulator of squamous differentiation, ΔNp63, is not activated upon *Foxa1/2* deletion, either *in vivo* (Figure 3F) or *in vitro* (data not shown). Moreover, acute deletion of *Foxa1/2* does not directly lead to a squamous morphology *in vivo* (Figure 1A). Taken together, these data show that that acute loss of FoxA1/2 induces genes that are highly expressed in the spinous and granular layers of the stratified squamous epithelia. We speculate that the absence ΔNp63 precludes a full squamous transdifferentiation in these cells.

Overall, these results illustrate that FoxA1/2 are critical transcriptional regulators of cellular identity in LUAD. FoxA1/2 are required for simultaneous expression of pulmonary and gastric programs, a mixed-lineage state important for LUAD disease progression as characterized by Marjanovic et al[50]. Loss of FoxA1/2 activates gene expression programs associated with stress-response, AT1/AT2, EMT, and maturing squamous epithelium. In pancreatic cancer, FoxA1/2 loss also promotes EMT[52]. Despite the fact that EMT is often associated with cancer progression, increased expression of the EMT transcriptional program is not sufficient to enhance proliferation in this context. Instead, it appears that additional factors dominate the outcome of FoxA1/2 loss and have a net inhibitory effect on tumor growth. This is likely the cumulative result of multiple cellular transitions including: (1) loss of mixed-lineage identity, (2) induction of a transcriptional program found in terminally differentiating stratified squamous epithelia, and (3) activation of an AT1/AT2 mixed identity program.

NKX2-1 impairs tumor growth in the absence of FoxA1/2

Although *Foxa1/2* deletion severely inhibited LUAD growth and extended survival (Figure 1D), a small number of tumors in KPF_1F_2 mice grew to macroscopic size despite the absence of FoxA1/2. Histopathological analysis showed that macroscopic FoxA1/2-negative tumors fell into two distinct classes. The first class consists of poorly differentiated, high grade tumors that lose NKX2-1 expression (Figure 4A). The second class is characterized by a keratinizing squamous cell carcinoma (SCC) morphology and stochastic activation expression ΔNp63. These SCCs retain expression of NKX2-1, albeit at reduced levels compared to adenocarcinomas (Supplemental Figure 4A). These data raise the possibility that loss of NKX2-1 and/or activation of ΔNp63 might enable LUAD to overcome *Foxa1/2* deletion. Consistent with the first possibility, subcutaneous tamoxifen-treated tumors also decreased NKX2-1 levels and adopted a quasi-mesenchymal morphology as they recovered from initial tumor regression caused by *Foxa1/2* deletion (Figure 2D, right column).

We used multiple independent approaches to determine whether loss of NKX2-1 is sufficient to rescue *Foxa1/2* deletion. First, we initiated $Kras^{G12D}$-driven p53-proficient tumors, allowed tumors to develop for 6 weeks, and then administered tamoxifen to delete *Foxa1* alone (KF_1), *Foxa1* and *Foxa2* (KF_1F_2), *Nkx2-1* alone (KN), or *Nkx2-1, Foxa1* and *Foxa2* (KNF_1F_2). Tumors progressed for an additional 6 weeks before tissue was collected. *Nkx2-1* deletion significantly rescued the effects of *Foxa1/2*-deletion on overall tumor burden, which was almost as high in KNF_1F_2 mice as in KN mice (Fig 4B). We have previously shown that KNF_1F_2 mice develop two distinct tumor types (squamocolumnar junction (SCJ)-like and keratinizing squamous cell carcinoma (SCC), also pictured in Supplemental Figure 4B)[10]. Both subtypes contributed to the overall increase in tumor burden of KNF_1F_2 mice (individual subtypes quantified in Supplemental Figure 4C) and are more proliferative than KF_1F_2 tumors (Figure 4C). SCC lesions have a higher BrdU incorporation rate than SCJ-like lesions, consistent with the fact that SCC can form macroscopic tumors whereas SCJ-like lesions remain microscopic in size.

We also introduced an shRNA against NKX2-1[14] to our KPF_1F_2 cell lines and organoids in order to decrease NKX2-1 levels alongside deletion of *Foxa1/2* via 4-OHT treatment (Figure 4D&F). Knockdown of NKX2-1 partially rescues the proliferation defect observed upon *Foxa1/2* deletion in both 2D cell lines (Figure 4E) and organoid cultures (Figure 4G). (As expected from previous work[12,14], NKX2-1 knockdown also enhances proliferation in

parental FoxA1/2-positive cell lines and organoids.) In order to determine whether NKX2-1 knockdown prevents tumor regression upon FoxA1/2 loss, we subcutaneously injected NSG mice with the 3311 cell line carrying shNKX2-1 and treated mice with either vehicle or tamoxifen when tumors reached an average volume of 200mm^3. We found that NKX2-1 knockdown increases the rate of growth in both the tamoxifen and vehicle treatments, and that NKX2-1 knock down prevents tumor regression seen in the shScramble tamoxifen treated cohort (Figure 2 D-E, Figure 4 H, Supplemental Figure 4 D-E.)

Together, these results demonstrate that NKX2-1 restrains tumor growth in the absence of FoxA1/2. We have previously shown that NKX2-1 regulates FoxA1/2 genome localization activity[12]. We hypothesize that in the absence of FoxA1/2, NKX2-1 localizes to new regions of the genome and activates growth inhibitory gene expression programs. NKX2-1 regulates specific gene expression programs in normal AT2 and AT1 cells[53,54]. We speculate that an NKX2-1-driven AT1-like program activated in the absence of FoxA1/2 might be less compatible with tumorigenesis than the AT2-like program normally activated by NKX2-1 in the presence of FoxA1/2.

In summary, we have shown that NKX2-1 positive LUAD is dependent on FoxA1/2. Additionally, FoxA1/2 are necessary for the presence of the mixed-lineage state in LUAD progression and suppress AT1/AT2 and stratified squamous epithelial transcriptional programs. We hypothesize that both of those transcriptional programs contribute to antiproliferative phenotypes associated with FoxA1/2 loss. Furthermore, we have shown that even though NKX2-1 requires FoxA1/2 at canonical pulmonary marker genes in LUAD, NKX2-1 retains some degree of tumor suppressive activity in the absence of FoxA1/2. Future studies will examine how FoxA1/2 regulate NKX2-1 localization and transcriptional activity in order to identify the mechanism(s) by which NKX2-1 inhibits tumorigenesis in the absence of FoxA1/2. We also anticipate that NKX2-1 interacts with distinct transcription factors and co-factors in the presence and absence of FoxA1/2. Although transcription factors have been historically viewed as undruggable, recent advances in targeted degradation have the potential to make transcription factor inhibition a pharmacologically tractable strategy in cancer[55]. This study outlines potential response to targeted degradation or pharmacological inhibition of FoxA1/2 transcriptional activity, and identifies candidate resistance mechanisms by which tumors can overcome the loss of FoxA1/2. More broadly, identifying

the master transcriptional regulators of cellular identity and investigating the impact of their inactivation is critical for understanding of mechanisms of cancer progression and will contribute to the development of differentiation state-specific therapeutic strategies.

Acknowledgements: We are grateful to members of the Snyder lab for suggestions and comments. We thank Brian Dalley for sequencing expertise and James Marvin for FACS expertise, and University of Utah core facilities (PRR, BMP, DNA sequencing, Genomics/Bioinformatics, Flow Cytometry). ELS was supported grants from NIH (R01CA212415 and R01CA240317), a Career Award for Medical Scientists from the Burroughs Wellcome Fund, and institutional funds (Department of Pathology and Huntsman Cancer Institute/Huntsman Cancer Foundation, University of Utah). GO was supported by the NIH (F31CA243427 and the Eunice Kennedy Shriver National Institute of Child Health & Human Development of the National Institutes of Health under Award Number T32HD007491). Research reported in this publication utilized shared resources (including Flow Cytometry, High Throughput Genomics, Bioinformatics, and Biorepository and Molecular Pathology) at the University of Utah and was supported by the National Cancer Institute of the National Institutes of Health under Award Number P30CA042014. Work in the flow cytometry core was also supported by the National Center for Research Resources of the National Institutes of Health under Award Number 1S20RR026802. The content is solely the responsibility of the authors and does not necessarily represent the official views of the NIH.

Competing interests: None

Author contributions: GO and ES designed experiments. GO, AJ, and KG performed experiments. GO, BL, and ES analyzed data. ES performed histopathologic review. GO and ES wrote the manuscript. All authors discussed results, reviewed and revised the manuscript.

FIGURES

Figure 1: FoxA1/2 are required for growth of NKX2-1-positive lung adenocarcinoma *in vivo*.

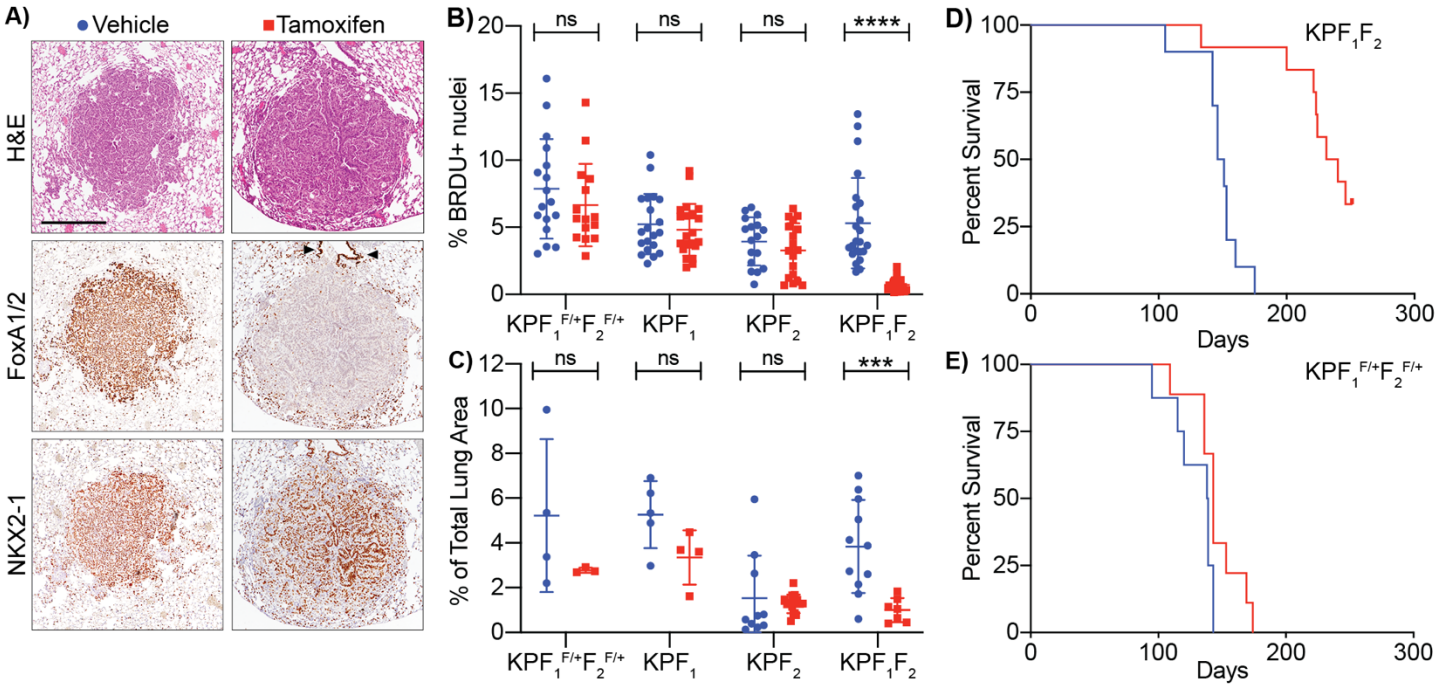

A) Representative images of KPF_1F_2 tumors 8 weeks post-initiation with adenoviral CMV-FlpO. Tamoxifen or vehicle administered 6 weeks post-initiation. IHC for FoxA1/2 and NKX2-1 and Hematoxylin and Eosin (H&E) staining shown. Arrowheads in upper right panel showing positive FoxA1/2 signal within airways, confirming tumor-specific deletion of FoxA1/2 (scale bar 1000 μm).

B) BRDU IHC quantification of individual $KPF_1^{F/+}F_2^{F/+}$, KPF_1, KPF_2, and KPF_1F_2 tumors initiated with adenoviral CMV-FlpO, injected with tamoxifen (red) or vehicle (blue) 6 weeks later, and sacrificed at 8 weeks (1 hour post BRDU injection; ****$p<0.0001$, unpaired t-test)

C) Tumor burden quantification of individual mice from the experiment shown in B (***$p=0.001014$, unpaired t-test)

D) KPF_1F_2 survival study in which tamoxifen (red, n=12) or vehicle (blue, n=10) was administered 10 weeks post-initiation with lentiviral EFS-FlpO (vehicle median survival of 21.21 weeks; tamoxifen median survival of 34.71 weeks; $p<0.0001$, Log-rank Mantel-Cox test).

E) $KPF_1^{F/+}F_2^{F/+}$ survival study in which tamoxifen (red, n=9) or vehicle (blue, n=8) was administered 10 weeks post-initiation with lentiviral EFS-FlpO (vehicle median survival of 19.79 weeks; tamoxifen median survival of 20.43 weeks; $p=0.0645$, Log-rank Mantel-Cox test).

Supplemental Figure 1

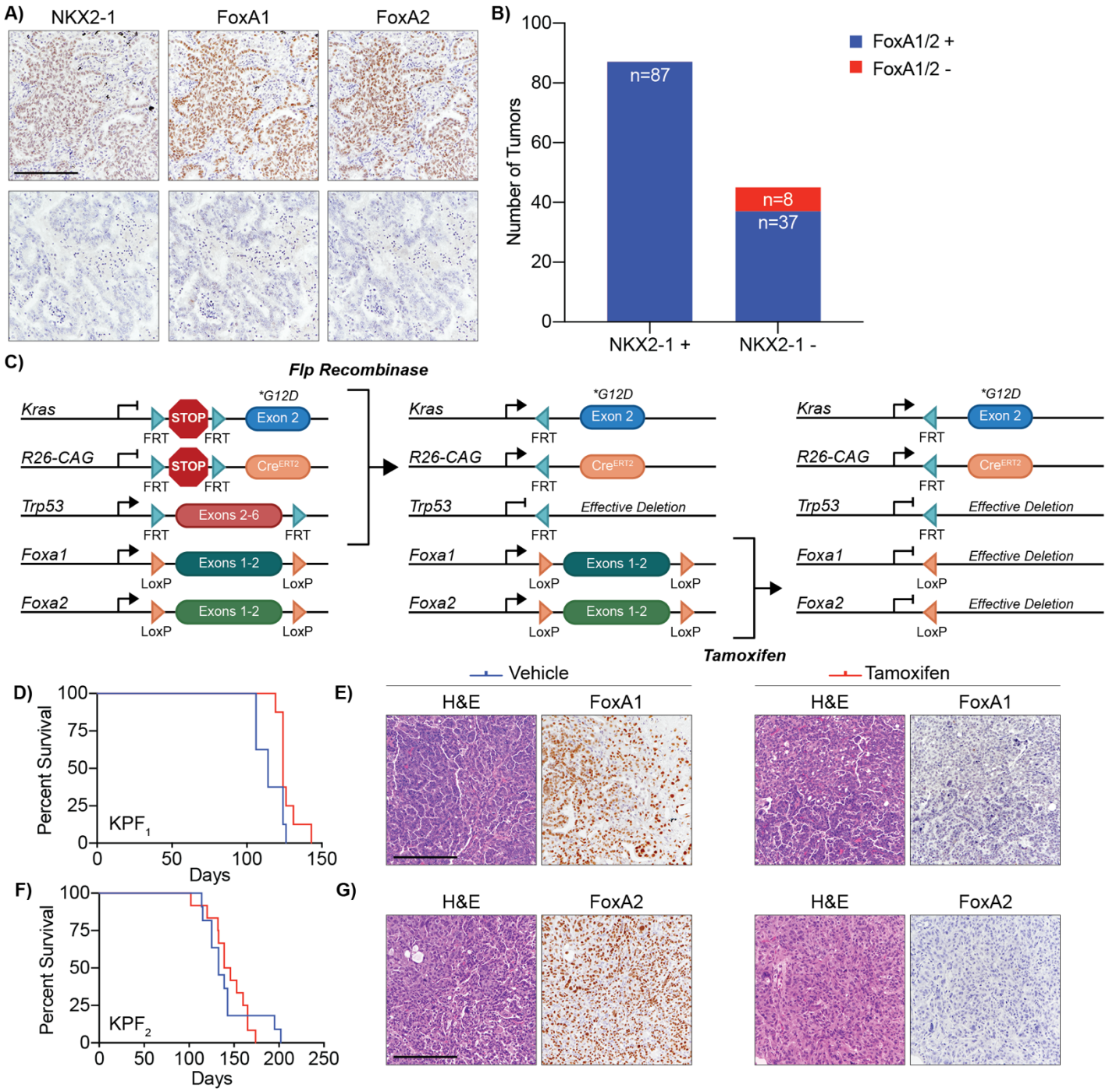

A) Representative IHC images from human tissue microarrays illustrating that NKX2-1-positive tumors retain FoxA1/2 expression while NKX2-1-negative tumors can lose FoxA1/2 expression (scale bar 500 μm).

B) Histological analysis of human tumors. All NKX2-1 positive LUAD tumors evaluated (n=87) express FoxA1 and/or FoxA2. FoxA1 and/or FoxA2 were detected in 82% (37/45) of tumors NKX2-1-negative LUAD tumors evaluated, while there was no detectable FoxA1 or FoxA2 expression in 18% (8/45) NKX2-1-negative tumors. ($p<0.0001$, Fisher's Exact test).

C) KPF_1F_2 mouse model. Mice are intubated with viral FlpO recombinase, which activates the expression of oncogenic $KRAS^{G12D}$ and Cre^{ERT2} and deletes *Trp53* in normal lung epithelial cells. This initiates the development of tumors in which Cre^{ERT2} is expressed, but sequestered to the cytoplasm. After tumors have developed we inject mice with tamoxifen, which allows Cre^{ERT2} to enter the nucleus exclusively in tumor cells and delete FoxA1 and FoxA2.

D) KPF_1 survival study in which tamoxifen (red, n=8) or vehicle (blue, n=8) was administered 10 weeks post-initiation with lentiviral EFS-FlpO (vehicle median survival of 16.29 weeks; tamoxifen median survival of 17.71 weeks; p=0.0290, Log-rank Mantel-Cox test).

E) Representative H&E and IHC images from the KPF_1 survival study shown in D (scale bar 500 μm).

F) KPF_2 survival study in which tamoxifen (red, n=12) or vehicle (blue, n=11) was administered 10 weeks post-initiation with lentiviral EFS-FlpO (vehicle median survival of 19.00 weeks; tamoxifen median survival of 20.36 weeks; p=0.9499, Log-rank Mantel-Cox test).

G) Representative H&E and IHC images from the KPF_2 survival study shown in F (scale bar 500 μm).

Figure 2: FoxA1/2 are required for growth of NKX2-1-positive lung adenocarcinoma *in vitro*.

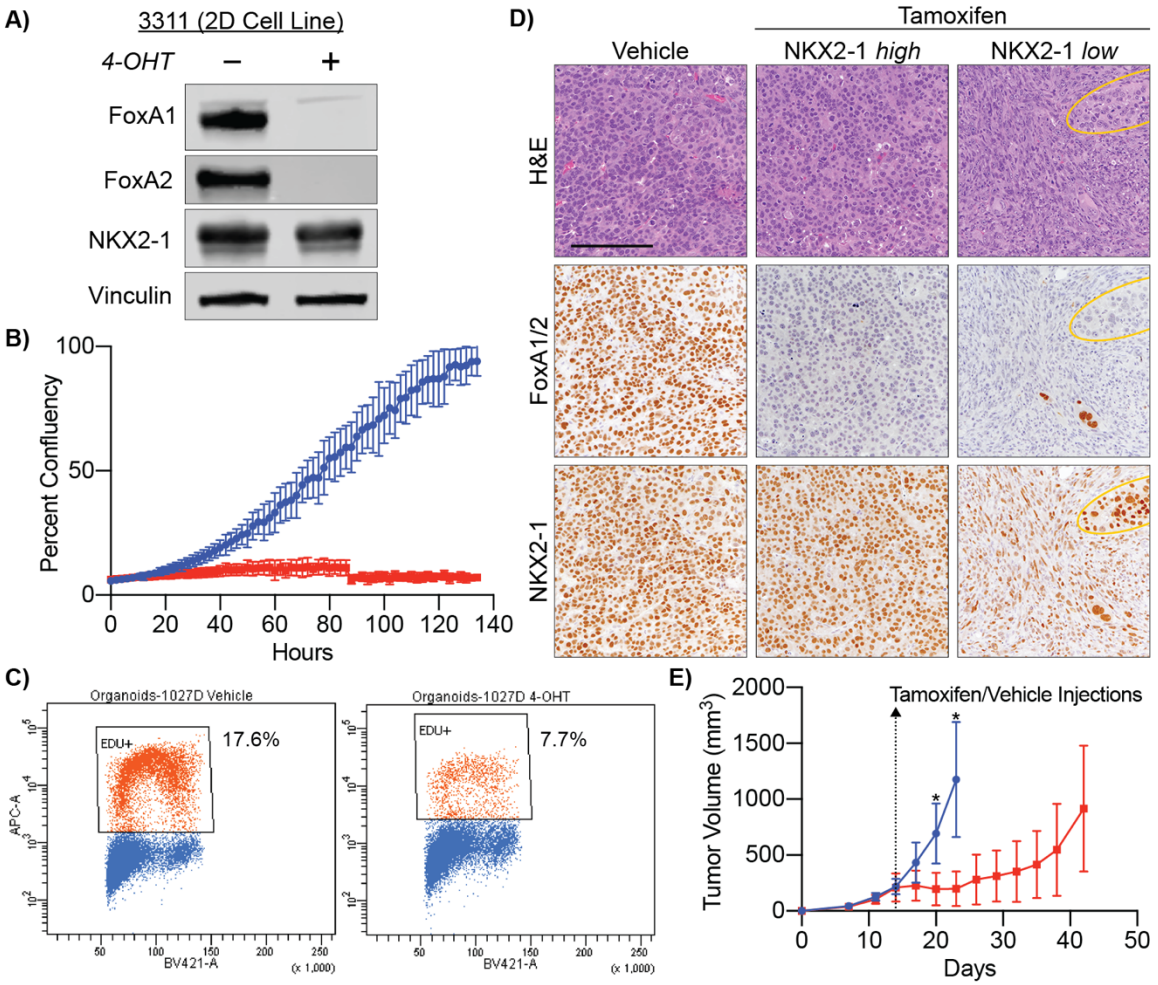

A) Western blot of protein extract from 2D KPF_1F_2 cell line (3311) collected 3 days post 48-hour 4-hydroxytamoxifen (4-OHT) treatment demonstrating complete loss of FoxA1/2.

B) Incucyte-based confluency growth assay of 3311 treated with vehicle (blue) or 4-OHT (red) one week before seeding 7,000 cells/well (n=3 biological replicates with 8 technical replicates each; $p<0.0001$ unpaired t-test of endpoint values).

C) Representative EDU-incorporation proliferation assay flow cytometry plots of 1027D KPF_1F_2 organoid line one week post 72-hour treatment with vehicle (left) or 4-OHT (right; BV421-A is DAPI; APC-A is EDU; n=2 biological replicates).

D) Representative images of subcutaneous tumors from experiment shown in E. H&E and IHC for FoxA1/2 and NKX2-1. Tamoxifen-treated tumors yielded two phenotypes: NKX2-1-high tumors with similar morphology to FoxA1/2-positive tumors and NKX2-1-low tumors with sarcomatoid/quasi-mesenchymal morphology (NKX2-1-high region outlined in yellow; scale bar 500 μm).

E) Subcutaneous tumors (3311 cell line) were allowed to grow to an average of $200mm^3$ before treating with either vehicle (n=8) or tamoxifen (n=11) and progressed until one tumor from the treatment cohort surpassed $1000mm^3$ (unpaired t-test, $*p<0.0001$).

Supplemental Figure 2

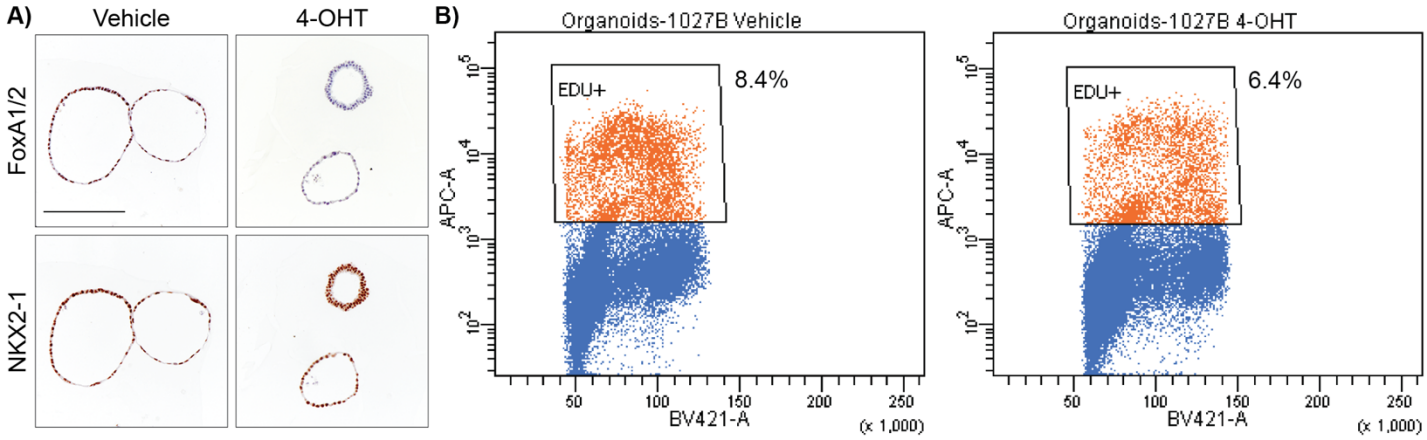

A) IHC for FoxA1/2 and NKX2-1 in KPF_1F_2 organoid line 1027B collected 3 days post 72-hour treatment with 4-OHT or vehicle demonstrating complete loss of FoxA1/2 (scale bar 500 μm).

B) Representative EDU-incorporation proliferation assay flow cytometry plots of 1027B KPF_1F_2 organoid line one week post 72-hour treatment with vehicle (left) or 4-OHT (right; BV421-A is DAPI; APC-A is EDU; n=2 biological replicates).

Figure 3: FoxA1/2 regulate multiple differentiation programs in NKX2-1-positive lung adenocarcinoma.

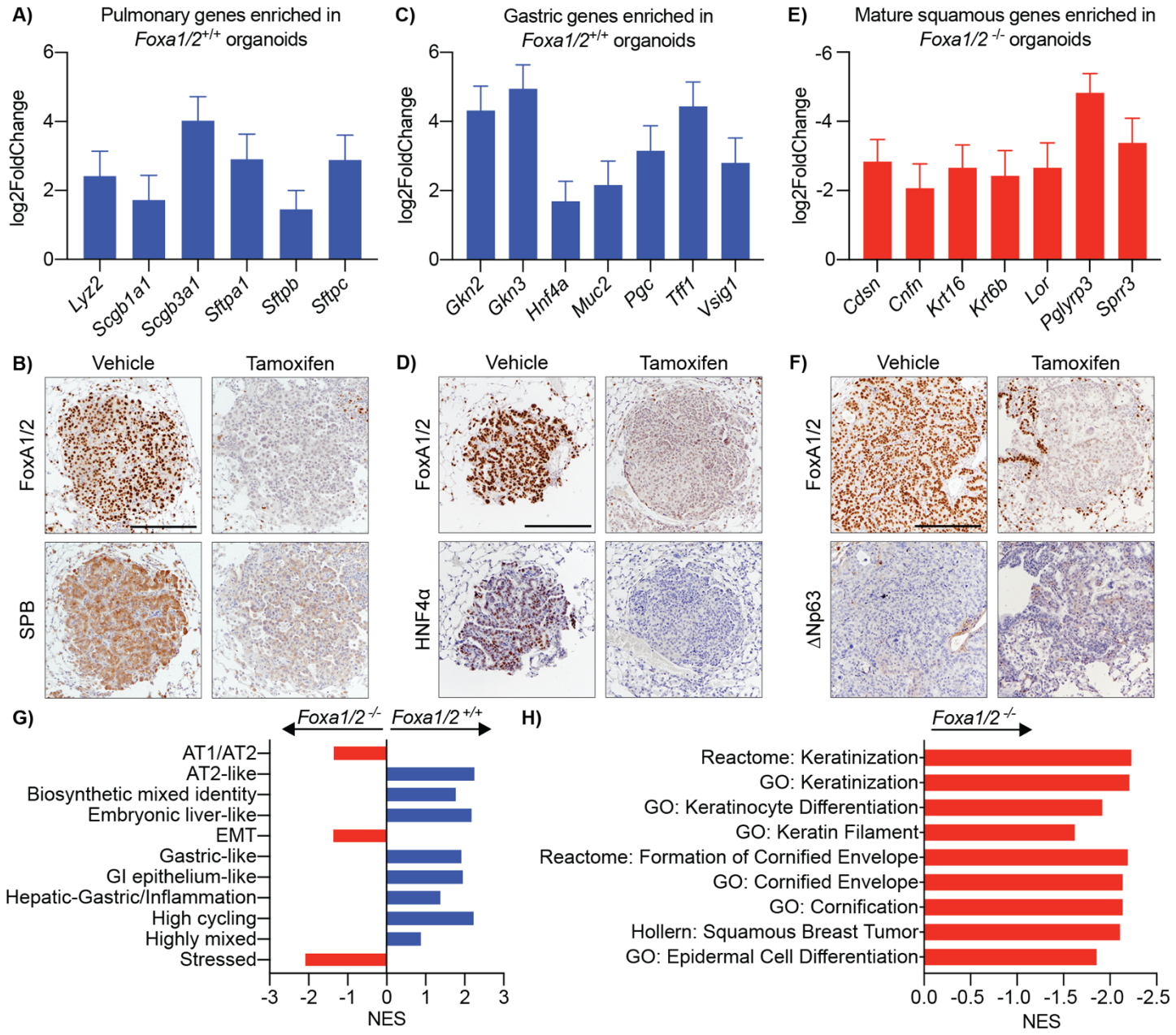

A) Log2FoldChange values determined by DESeq2 for select pulmonary markers enriched in FoxA1/2-positive organoids.

B) Representative IHC images of pulmonary marker SPB in FoxA1/2-positive and FoxA1/2-negative tumors, illustrating the loss of pulmonary lineage upon *Foxa1/2* deletion (scale bar 500 μm).

C) Log2FoldChange values determined by DESeq2 for select gastric markers enriched in FoxA1/2-positive organoids.

D) Representative IHC images of gastric marker HNF4α in FoxA1/2-positive and FoxA1/2-negative tumors, illustrating the loss of gastric lineage upon *Foxa1/2* deletion (scale bar 500 μm).

E) Log2FoldChange values determined by DESeq2 for select squamous markers enriched in FoxA1/2-negative organoids.

F) Representative IHC images of ΔNp63 in FoxA1/2-positive and FoxA1/2-negative tumors, illustrating the lack of expression in both tumor types (scale bar 500 μm).

G) Gene Set Enrichment Analysis (GSEA) intersecting the differentially expressed genes identified in KPF_1F_2 organoid RNAseq with the 11 transcriptional programs in KP murine LUAD as defined by Marjanovic et al[50] (NES=Normalized Enrichment Score)

H) NES of representative gene sets associated with a squamous differentiation from GSEA intersection of the differentially expressed genes identified in KPF_1F_2 organoid RNAseq with all available MSigDB gene set collections.

Supplemental Figure 3

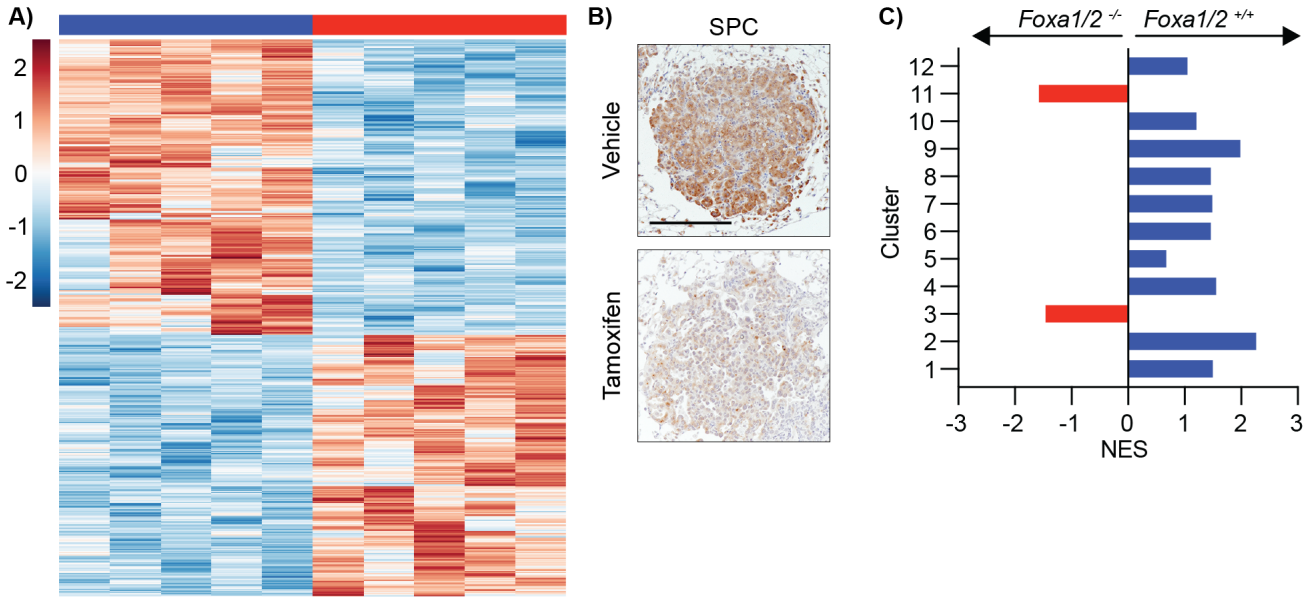

D)

Program	NES	FDR
AT1/AT2	-1.358589	0.0219808
AT2-Like	2.249282	0
Biosynthetic Mixed Identity	1.7729167	0
Embryonic liver-like	2.1783412	0
EMT	-1.3737977	0.027164
Gastric-like	1.9162276	0
GI Epithelium-like	1.9517804	0
Hepatic-Gastric/Inflammation	1.3782303	0.011566
High Cycling	2.2304318	0
Highly Mixed	0.8755122	0.8301233
Stressed	-2.0960994	0

Cluster	NES	FDR
Cluster 1	1.5024518	0.01126609
Cluster 2	2.2677662	0
Cluster 3	-1.4636143	0.0040895
Cluster 4	1.5645154	0.00685503
Cluster 5	0.6807365	0.99157727
Cluster 6	1.4666723	0.01231351
Cluster 7	1.4933571	0.01044349
Cluster 8	1.472231	0.01376967
Cluster 9	1.9907401	0
Cluster 10	1.2197796	0.08074031
Cluster 11	-1.5802107	0.00174293
Cluster 12	1.0597987	0.31222028

A) Three KPF_1F_2 organoid lines (1027B, 1027D, and 1292B) were treated with 4-OHT or vehicle for 72 hours, and then cultured for three weeks before two biological replicates of RNA were collected per line and condition and sequenced. We identified 802 differentially expressed genes: 400 enriched in FoxA1/2-positive organoids (upper blue bar) and 402 enriched in FoxA1/2-negative organoids (upper red bar).

B) Representative IHC images of pulmonary marker SPC in FoxA1/2-positive (vehicle) and FoxA1/2-negative (tamoxifen) tumors, illustrating the loss of pulmonary lineage upon FoxA1/2 deletion (scale bar 500 μm).

C) GSEA intersection of the differentially expressed genes identified in KPF_1F_2 organoid RNAseq with the 12 clusters in KP murine LUAD as defined by Marjanovic et al[50] (NES=Normalized Enrichment Score).

D) Normalized Enrichment Score and False Discovery Rate calculated by GSEA when intersecting the differentially expressed genes identified in KPF_1F_2 organoid RNAseq with the 11 transcriptional programs and 12 clusters in KP murine LUAD as defined by Marjanovic et al[50] (Non-significant results in grey).

Figure 4: NKX2-1 restrains tumor growth in the absence of FoxA1/2

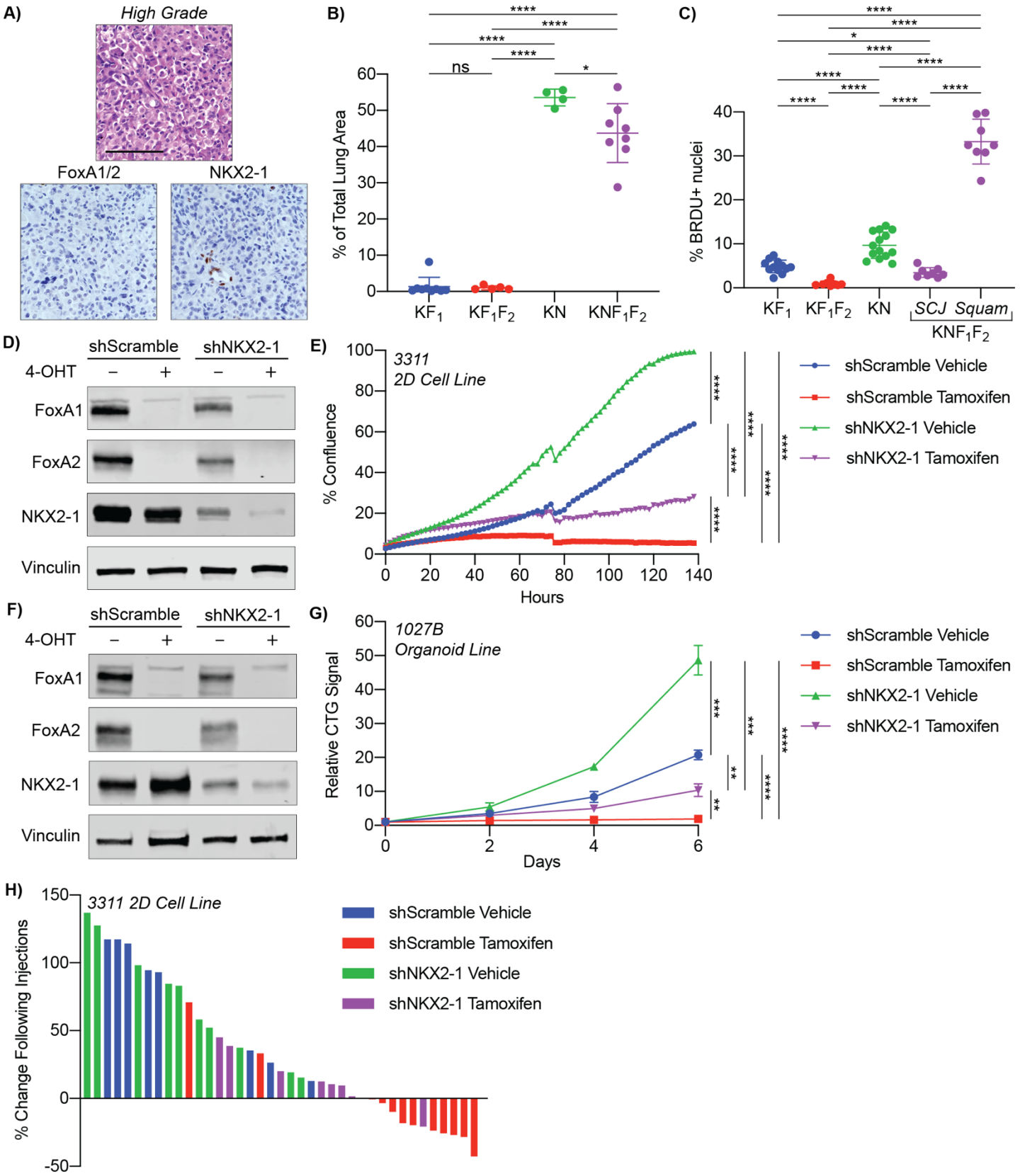

A) Representative images of high grade, NKX2-1-negative tumors that emerged in the FoxA1/2-negative cohort of long term survival studies. Top panel H&E, bottom panels IHC (scale bar 250 μm).

B) Tumor burden quantification of KF_1, KF_1F_2, KN, and KNF_1F_2 tumors initiated with adenoviral SPC-Flp, injected with tamoxifen 6 weeks later, and sacrificed at 12 weeks (multiple unpaired t-tests; *p=0.0424; ****p<0.0001).

C) BRDU IHC quantification experiment shown in B (multiple unpaired t-tests; *p=0.0366; ****p<0.0001)

D) Western blot of protein extract from standard culture KPF_1F_2 cell line (3311) transduced with shScramble and shNKX2-1 collected 3 days post 48-hour 4-OHT/vehicle treatment demonstrating successful knock down of NKX2-1.

E) Incucyte-based confluency growth assay of cells shown in D one week after 4-OHT/vehicle treatment. One representative experiment shown of two biological replicates with 8 technical replicates each (multiple unpaired t-tests of endpoint values; ****p<0.0001).

F) Western blot of 1027B organoids transduced with shScramble and shNKX2-1 collected post 72-hour 4-OHT/vehicle treatment demonstrating successful knock down of NKX2-1.

G) Timecourse experiment using the CellTiter-Glo 3D cell viability assay of cells shown in F. CTG assay was performed on the day of seeding, as well as 2, 4, and 6 days post-seeding. Data shown relative to day 0 luminescence reads for each condition. One representative experiment shown of two biological replicates with 3 technical replicates each (multiple unpaired t-tests of endpoint values; **p=0.0016; ***p<0.0005; ****p<0.0001).

H) Waterfall plot showing the % change in individual subcutaneous tumor volumes. Percent change representing the first measurement post-tamoxifen/vehicle injections relative to the measurement immediately preceding treatment.

Supplemental Figure 4

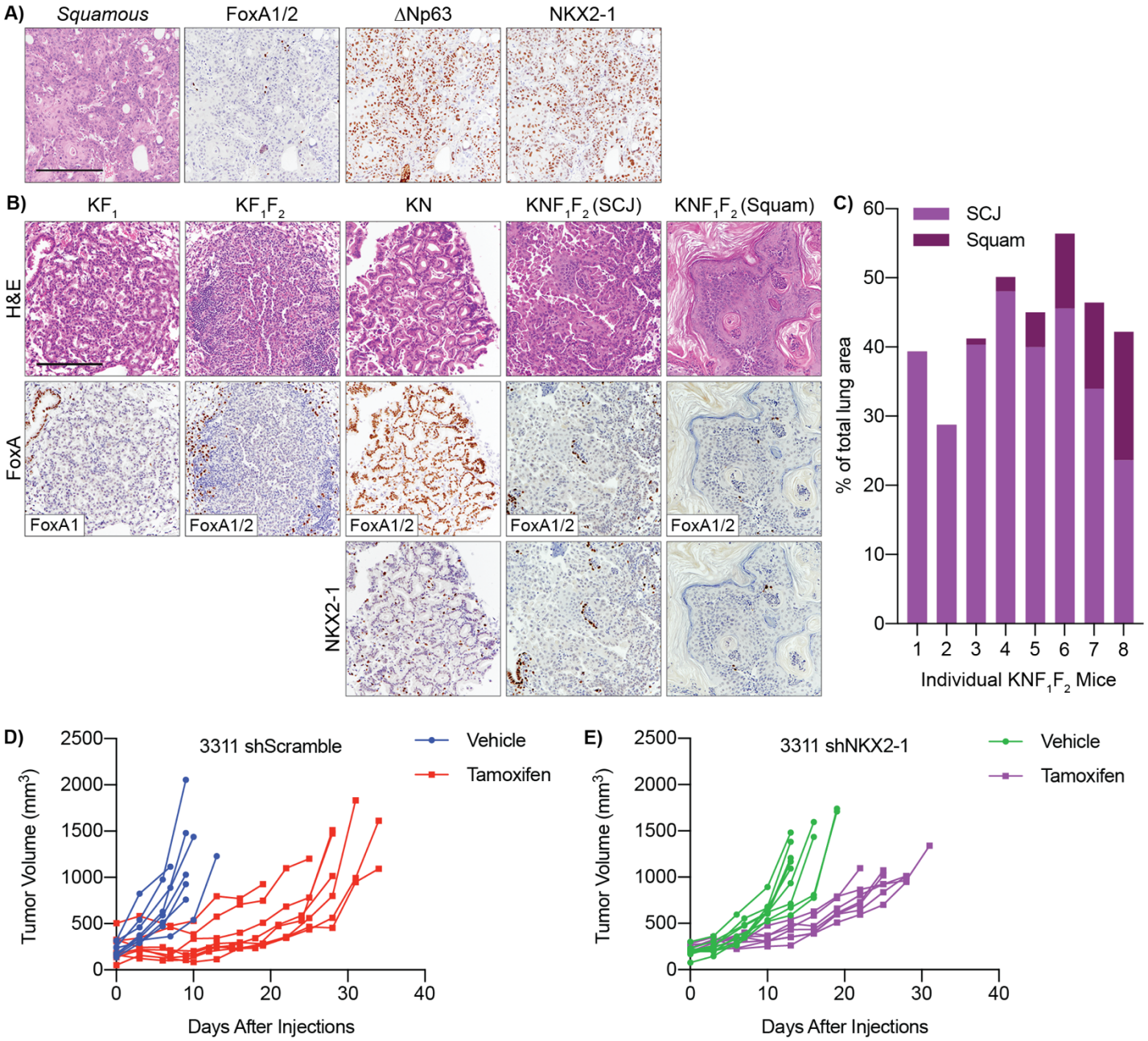

A) Representative images of squamous, ΔNp63-positive, NKX2-1-positive tumors that emerged in the FoxA1/2-negative cohort of long term KP survival studies (scale bar 500 μm).

B) Representative images of KF_1, KF_1F_2, KN, and KNF_1F_2 tumors in which alleles were deleted via tamoxifen treatment 6 weeks post-tumor initiation, and tissue was collected 12 weeks post-tumor initiation (SCJ=Squamocolumnar Junction; Squam=Squamous; scale bar 500 μm).

C) Percentage of tumor burden in individual KNF_1F_2 mice attributable to SCJ and Squamous phenotypes.

D) Measurements of subcutaneous tumor volume for individual mice allografted with 3311 shScramble and injected with vehicle or tamoxifen. Each line represents an individual tumor.

E) Measurements of subcutaneous tumor volume for individual mice allografted with 3311 shNKX2-1 and injected with vehicle or tamoxifen. Each line represents an individual tumor.

Supplemental Tables

Table 1: Detailed histological analysis of $KPF_1^{F/+}F_2^{F/+}$, KPF_1, KPF_2, and KPF_1F_2 survival studies

Table 2: Differentially expressed genes in KPF_1F_2 organoid isogenic pairs as determined by DEseq2

Table 3: Significantly enriched gene sets in KPF_1F_2 organoid isogenic pairs as determined by GSEA

METHODS

Mice, tumor initiation, tamoxifen administration, and BrdU administration *in vivo*

Mice harboring *Kras*$^{FSF\text{-}G12D}$ [45], *p53*^{frt} [46], *Rosa-FSF-Cre*^{ERT2} [47], *Foxa1*^{flox} [31], and *Foxa2*^{flox} [48] have been previously described. All animals were maintained on a mixed 129/B6 background. Animal studies were approved by the IACUC of the University of Utah, conducted in compliance with the Animal Welfare Act Regulations and other federal statutes relating to animals and experiments involving animals, and adhered to the principles set forth in the Guide for the Care and Use of Laboratory Animals, National Research Council (PHS assurance registration number A-3031-01).

Autochthonous lung tumors were initiated by administering viruses via intratracheal intubation. Adenoviruses were obtained from University of Iowa Viral Vector Core. Lentivirus was generated as described in **Lentiviral production and transduction** methods section.

Experiment	**Virus**	**PFU/mouse**
Figure 1A-C	Adeno-CMV-FlpO	$4x10^7$
Figure 1D-E, 4A; Supplemental Figure 1 D-G, 4A	Lenti-EFS-FlpO	$1x10^4$
Figure 4B-C; Supplemental Figure 4 B-C	Adeno-mSPC-FlpO	$1x10^9$

Tumor-specific activation of CreER^{T2} nuclear activity was achieved by intraperitoneal injection of tamoxifen (Sigma) dissolved in corn oil at a dose of 120mg/kg. Mice received 4 injections over the course of 5 days. For survival experiments, mice were additionally given pellets supplemented with 500mg/kg tamoxifen (Envigo). BrdU incorporation was performed by injecting mice at 40 mg/kg (Sigma) intraperitoneally 1 hour prior to tissue collection. Mice in survival studies were monitored for lethargy and respiratory distress, at which time animals were euthanized.

Analysis of primary human lung adenocarcinoma

Whole sections of de-identified formalin fixed, paraffin-embedded (FFPE) LUAD (n=42) were obtained from the Intermountain Biorepository, which collects samples in accordance with protocols approved by the Intermountain

Healthcare Institutional Review Board. An additional 92 de-identified tumors were evaluated by FFPE tissue microarrays obtained from US Biomax (BC04115c and BCS04017).

Histology and immunohistochemistry

All tissues were fixed in 10% formalin overnight and when necessary, lungs were perfused with formalin via the trachea. Organoids were first fixed in 10% formalin overnight and then mounted in HistoGel (Thermo Fisher Scientific). Mounted organoids and tissues were transferred to 70% ethanol, embedded in paraffin, and four-micrometer sections were cut. Immunohistochemistry (IHC) was performed manually on Sequenza slide staining racks (Thermo Fisher Scientific). Sections were treated with Bloxall (Vector Labs) followed by Horse serum 536 (Vector Labs) or Rodent Block M (Biocare Medical), primary antibody, and HRP-polymer-conjugated secondary antibody (anti-Rabbit, Goat and Rat from Vector Labs; anti-Mouse from Biocare. The slides were developed with Impact DAB (Vector Labs) and counterstained with hematoxylin. Slides were stained with antibodies to FoxA1 (1:4000, Abcam 10881-14), FoxA2 (1:1200, Abcam 4466), Murine NKX2-1 (1:2000, Abcam EP1584Y), Human NKX2-1 (1:2000, Abcam 133638), BRDU (1:400, Abcam BU1/75), proSP-B (1:3000, Millipore AB3430), proSP-C (1:4000, Millipore AB3786), HNF4α (1:500, CST C11F12), ΔNp63 (1:100, Biocare [clone BC28]). Pictures were taken on a Nikon Eclipse Ni-U microscope with a DS-Ri2 camera and NIS-Elements software. Tumor Burden and BrdU quantitation and histological analyses were performed on hematoxylin and eosin-stained and IHC-stained slides using NIS-Elements software. All histopathologic analysis was performed by a board-certified anatomic pathologist (E.L.S.).

Establishing primary murine LUAD cell lines and organoids

Five months after tumor initiation in KF_1F_2 mice (2D cell lines; Lenti-CA2-FlpO-sh*p53*) and KPF_1F_2 mice (3D organoid lines; Adeno-mSPC-FlpO), tumor bearing mice were euthanized and lungs were isolated. Individual macroscopic tumors were removed from lungs, minced under sterile conditions, and digested at 37°C for 30 minutes with continuous agitation in a solution of Advanced DMEM/F12 containing the following enzymes: Collagen Type I (Thermo Fisher Scientific, 450U/ml), Dispase (Corning, 5U/ml), DNaseI (Sigma, 0.25mg/ml). Enzyme reactions were stopped by addition of cold DMEM/F-12 with 10% FBS. The digested tissue was

repeatedly passed through a 20-gauge syringe needle, sequentially dispersed through 100μm, 70 μm, and 40μm cell strainers, and treated with erythrocyte lysis buffer (eBioscience) to obtain a single cell suspension.

Standard cultures were established by seeding tumor cells in adherent culture flasks. Organoid cultures were established by seeding $1x10^5$ tumor cells in 50ul of Matrigel (Corning) and plated in 24-well plates. For the first 1-2 weeks of organoid initiation, Matrigel droplets were overlaid with recombinant organoid medium: Advanced DMEM/F-12 supplemented with 1X B27 (Gibco), 1X N2 (Gibco), 1.25mM nAcetylcysteine (Sigma), 10mM Nicotinamide (Sigma), 10nM Gastrin (Sigma), 100ng/ml EGF (Peprotech), 100ng/ml R-spondin1 (Peprotech), 100ng/ml Noggin (Peprotech), and 100ng/ml FGF10 (Peprotech). After organoids were established, cultures were switched to 50% L-WRN conditioned media[56].

Organoid cultures were screened via immunohistochemistry and qPCR, and lines that uniformly expressed FoxA1, FoxA2, and NKX2-1 in all cells were selected for subsequent analysis. Standard culture cell lines were heterogeneous for NKX2-1, with both NKX2-1-positive and NKX2-1-negative cells identified within the same parental culture. In order to generate uniform cultures for downstream analysis our 2D cell lines were single cell cloned. The clonal populations were screened via immunoblotting for FoxA1, FoxA2, and NKX2-1, and the cell line with strongest expression of all three transcription factors was selected for subsequent analysis. The full name of the 2D cell line in this paper labeled 3311 is 3311-Tumor 3-Subclone 1, which was shortened for clarity.

Cell culture

Standard culture murine cell lines and HEK293T cells were cultured in DMEM/10% FBS (Gibco). Murine organoids were cultured within Matrigel (Corning or Preclinical Research Shared Resource core facility) submerged in 50% L-WRN conditioned media. All cell lines were tested periodically for mycoplasma contamination. To maintain cell cultures mycoplasma free, all culture media were supplemented with 2.5 ug/ml Plasmocin. Cells were transiently treated with 2μM 4-hydroxytamoxifen (Cayman Chemical Company, dissolved in 100% Ethanol) or vehicle for 48 (standard culture) or 72 (organoid culture) hours to activate $CreER^{T2}$ nuclear activity and generate isogenic pairs.

Immunoblotting

Cells were lysed on ice for 20 minutes in RIPA buffer (50mM Tris HCl pH 7.4, 150 mM NaCl, 0.1 % (w/v) SDS, 0.5% (w/v) sodium deoxycholate, 1% (v/v) Triton X-100) plus complete protease phosphatase inhibitor cocktail (A32961, Thermo Fisher Scientific). Cells debris were pelleted for 15 minutes at 4 ºC and protein concentration was quantitated with the Coomassie (Bradford) Protein Assay (ThermoFisher Scientific). A total of 15μg (organoids) or 30μg (cell lines) of protein lysates were separated on Tris-Glycine (TGX) precast gels (BIO RAD) and transferred to nitrocellulose membranes (Thermo Fisher Scientific). Membranes were probed overnight with antibodies to FoxA1 (1:1000, Abcam 23738), FoxA2 (1:1000, Abcam 108422), NKX2-1 (1:2000, Abcam 133638), and Vinculin (1:20000, Abcam 129002). The next day membranes were probed with IRDye 800CW Goat anti-Rabbit IgG Secondary Antibody (1:20000, LI-COR) and imaged with a LI-COR Odyssey CLx and Image Studio Software.

Generating a single cell suspension from organoid cultures

Matrigel droplets containing organoid cells were broken down via repeated pipetting in Cell Recovery Solution (Corning, 500μl per Matrigel droplet). Cell Recovery Solution containing organoids was transferred to sterile conical tubes and submerged in ice for 20-30 minutes before centrifugation at 4°C (300-500G). Cell Recovery Solution supernatant was removed and the cell pellet was washed via resuspension in PBS followed by centrifugation. Cells were then resuspended in pre-warmed TrypLE Express Enzyme (Thermo Fisher Scientific) and incubated for 5-7 minutes at 37°C. TrypLE reaction was quenched via dilution with cold Splitting Media (Advanced DMEM/F-12 [Gibco], 10 mM HEPES [Invitrogen], 1X Penicillin-Streptomycin-Glutamine [Invitrogen]). Cells were centrifuged and then resuspended in a pre-warmed DNase solution (L-WRN media supplemented to a final concentration of 200U/ml DNase [Worthington], 2.5 mM $MgCl_2$, 500 μM $CaCl_2$) and incubated for 5-7 minutes at 37°C. Cells were centrifuged and washed in PBS before use.

Cell viability and growth assays

<u>EDU Incorporation Assay</u>: One week after 4-OHT/Ethanol treatment, Matrigel droplets containing isogenic organoid cells were incubated in L-WRN/100mM EdU for 30 minutes. EdU solution was then removed and droplets were washed with 500μl of warm PBS before generating a single cell suspension. The single cell

suspension was fixed in 1ml of PFA in PME Buffer for 20 minutes (4% Formaldehyde [Pierce], 500 mM PIPES, 25 mM $MgCl_2$, 50 mM EDTA in UltraPure Water [Invitrogen]), washed in 1ml of IF Buffer (PBS pH 7.4, 0.20% Triton X-100, 0.05% Tween-20), permeabilized for 20 minutes in 1X Click-iT Permeabilization and Wash Reagent (Thermo Fisher), washed in PBS/3% BSA, incubated shielded from light for 30 minutes in 500μl of Click-iT Reaction Cocktail (Thermo Fisher), washed in 3ml of 1X Click-iT Permeabilization and Wash Reagent, and resuspended in 500μl of DAPI Solution (1 μg/ml in 1X Click-iT Permeabilization and Wash Reagent). Cells were analyzed on a BD LSR Fortessa. Events first passed through routine light-scatter and doublet discrimination gates before being concurrently analyzed for DAPI signal for cell cycle distribution (BV421, Area) vs EdU signal for actively replicating cells (Alexa Fluor 647, Area). EdU-High cells were quantified as a percent of total population, and then the percentage of EdU-High 4-OHT-treated cells were normalized to the percentage of EdU-High isogenic Ethanol cells.

Incucyte Live-Cell Imaging: Standard culture cells were seeded at a density of 7,000 cells per well in a 96-well plate and grown within an IncuCyte Live Cell Imaging System. Wells were imaged every two hours. Percent phase confluence was determined using IncuCyte Zoom software. Each experiment shown is one representative phase confluence plot with 8 technical replicates of three total biological replicates. Culture media was changed as needed and the assay was ended once one of the conditions reached 100% confluency.

CellTiter-Glo Assay: Organoid cells were broken down into a single cell suspension. Four identical 48-well plates were seeded with three wells per condition (5000 cells/well in 15 ul of Matrigel). The following protocol was performed on the day of seeding, and every other day for 6 days following seeding. CellTiter-Glo 3D reagent (Promega) and 50% L-WRN media were warmed to room temperature. A working solution was prepared with a ratio of 1 part CTG:5 parts L-WRN. Media was removed from each well, 330 μl of CTG working solution was added to each well containing organoids and one empty well before shielding from light and incubating at room temperature for 30 minutes on a plate shaker at 500 RPM. After incubation CTG working solution was transferred to a clear-bottom, solid-wall 96 well plate (100ul/well; 3 wells/replicate; 3 replicates/sample). Luminescence was measured using an EnVision 2105 Multimode Plate Reader (Perkin Elmer). Luminescent signal for each condition was normalized to the corresponding Day 0 luminescence read.

Subcutaneous allografts

For subcutaneous allograft experiments, a single cell suspension of $3x10^5$ standard culture cells were mixed in a 1:1 volume with 50 μl of Matrigel. Cells were subcutaneously injected into the flank of NOD/SCID-gamma chain deficient mice (NSG). Tumor dimensions were measured with calipers, and tumor volume was calculated using the $(L \times W^2)/2$ formula. When the average volume of the tumors surpassed $200mm^3$, mice were randomized into Corn Oil or Tamoxifen cohorts (120mg/kg Tamoxifen). Mice received daily injections for 4 days. Tumor volume was monitored and measured every 3 days, and mice were euthanized once one tumor within the cohort surpassed $1000mm^3$ (Figure 1) or individually as their tumor volume surpassed $1000mm^3$ (Figure 4/4S).

Lentiviral production and transduction

Cloning of EFS-FlpO lentivector: We generated a pCDH-EFS-FlpO lentiviral vector by PCR amplifying the EFS (EF1a) promoter from the pCDH-Cre plasmid[57], digesting the purified PCR product with XbaI, and cloning into SnaBI-XbaI sites of pCDH-CMV-FlpO[10] via ligation with T4 DNA ligase. Correct identity and orientation of the construct was confirmed via Sanger sequencing.

In vivo use: HEK293T cells were transfected with EFS-FlpO-encoding lentiviral vector, Δ8.9 packaging vector, and VSV-G envelope vector mixed with TransIT-293 (Mirus). Virus-containing supernatant was collected 36, 48, 60, and 72 hours after transfection, and then ultracentrifuged at 25,000 RPM for 2 hours to concentrate virus for *in vivo* infection. The concentration of the final viral stock was determined using the mouse fibroblast FlpO-GFP reporter cell line 3TZ to determine Plaque Forming Units/μl (PFU).

In vitro use: HEK293T cells were transfected with pLKO.shNkx2-1 (Addgene Plasmid #32400) or pLKO.shScramble (Addgene Plasmid #1864) lentiviral vectors, Δ8.9 packaging vector, and VSV-G envelope vector mixed with TransIT-293 (Mirus). Virus-containing supernatant was collected 48, 60, and 72 hours after transfection, centrifuged to pellet floating HEK293T cells, and filtered using 0.45μm filters before storing long term at -80°C.

Standard culture cell lines were transduced by culturing with undiluted lentiviral media containing 8 μg/ml polybrene for 48 hours total, refreshing the media and polybrene at 24 hours. Three days after transduction ceased, cells were subjected to Puromycin selection to produce stable lines. For stable transduction of isogenic organoid pairs post-4OHT/Ethanol treatment, Matrigel domes containing organoids were resuspended in ice cold Splitting Media and centrifuged at 300G 4°C twice. Cells were then resuspended in TrypLE Express Enzyme (Thermo Fisher Scientific), incubated for 5 minutes at 37°C, and quenched with ice cold Splitting Media. Cell pellets were resuspended in a 1:1 mixture, by volume, of 50% L-WRN and lentiviral media with a final concentration of 8 μg/ml polybrene, 1X Y-27632 (ROCK inhibitor), 1X A83-01 (ALK inhibitor), and 1X SB431542 (ALK inhibitor). The cell suspension was then transferred to a 6-well plate and centrifuged at 1700 RPM for 1 hour at room temperature. After centrifugation, the plate was incubated at 37°C for 2 hours. Cells were collected (scraping the bottom of the plate when necessary), centrifuged, resuspended in Matrigel, seeded in 24-well plates, and cultured in 50% L-WRN supplemented with 1X Y-27632, 1X A83-01, and 1X SB431542 for 72 hours. Three days after transduction, inhibitor media was washed away and cells were subjected to Puromycin selection to produce stable lines.

RNA Sequencing

RNA was collected from biological replicates of isogenic organoid cultures 1027B, 1027D, and 1292B 3 weeks after 4-OHT/Ethanol treatment. RNA was isolated via Trizol-chloroform extraction followed by column-based purification. The aqueous phase was brought to a final concentration of 50% ethanol, and RNA was purified using the PureLink RNA Mini kit according to the manufacturer's instructions (ThermoFisher Scientific). Library preparation was performed using the Illumina TruSeq Stranded mRNA Library Prep with UDI (Illumina; poly(A) selection). Sequencing was performed using the NovaSeq 6000 (50 x 50 bp paired-end sequencing; 25 million reads per sample).

RNAseq Data Processing and Analysis

Mouse FASTA and GTF files were downloaded from Ensembl release 98 and a reference database was created using STAR version 2.7.2c[58] with splice junctions optimized for 50 base pair reads. Optical duplicates were removed from NovaSeq runs via Clumpify v38.34[59]. Reads were trimmed of adapters and aligned to the

reference database using STAR in two pass mode to output BAM file sorted by coordinates. Mapped reads were assigned to annotated genes in the GTF file using featureCounts version 1.6.3[60]. Non-coding features, histones, and ribosomal RNAs were removed and differentially expressed genes were identified using a 5% false discovery rate with DESeq2 version 1.30.1[61].

GSEA-Preranked was run with the differential gene list generated from DESeq2 and the following MSigDB gene sets: c2, c3, c4, c5, c6, c8, and Hallmarks on November 12, 2020. Gene sets smaller than 15 and larger than 500 were excluded from analysis. Marjanovic et al Clusters and Program gene lists and Zou et al Epidermal Cell Types gene lists were downloaded from their respective supplemental materials.

REFERENCES

1 Boumahdi, S. & de Sauvage, F. J. The great escape: tumour cell plasticity in resistance to targeted therapy. *Nat Rev Drug Discov* **19**, 39-56, doi:10.1038/s41573-019-0044-1 (2020).

2 Le Magnen, C., Shen, M. M. & Abate-Shen, C. Lineage Plasticity in Cancer Progression and Treatment. *Annu Rev Cancer Biol* **2**, 271-289, doi:10.1146/annurev-cancerbio-030617-050224 (2018).

3 Quintanal-Villalonga, A. *et al.* Lineage plasticity in cancer: a shared pathway of therapeutic resistance. *Nat Rev Clin Oncol* **17**, 360-371, doi:10.1038/s41571-020-0340-z (2020).

4 Meza, R., Meernik, C., Jeon, J. & Cote, M. L. Lung cancer incidence trends by gender, race and histology in the United States, 1973-2010. *PLoS One* **10**, e0121323, doi:10.1371/journal.pone.0121323 (2015).

5 Travis, W. D. *et al.* International association for the study of lung cancer/american thoracic society/european respiratory society international multidisciplinary classification of lung adenocarcinoma. *J Thorac Oncol* **6**, 244-285, doi:10.1097/JTO.0b013e318206a221 (2011).

6 Campos-Parra, A. D. *et al.* Relevance of the novel IASLC/ATS/ERS classification of lung adenocarcinoma in advanced disease. *Eur Respir J* **43**, 1439-1447, doi:10.1183/09031936.00138813 (2014).

7 Niederst, M. J. *et al.* RB loss in resistant EGFR mutant lung adenocarcinomas that transform to small-cell lung cancer. *Nat Commun* **6**, 6377, doi:10.1038/ncomms7377 (2015).

8 Russell, P. A. W., Z.; Wright, G.M.; Daniels, M.; Conron, M.; Williams, R.A. Does lung adenocarcinoma subtype predict patient survival?: A clinicopathologic study based on the new International Association for the Study of Lung Cnacer/American Thoracic Society/European Respiratory Society international multidisciplinary lung adenocarcinoma classification. *Journal of thoracic oncology: official publication of the International Association for the Study of Lung Cnacer*, 1496-1504 (2011).

9 Sun, Z. & Yang, P. Gene expression profiling on lung cancer outcome prediction: present clinical value and future premise. *Cancer Epidemiol Biomarkers Prev* **15**, 2063-2068, doi:10.1158/1055-9965.EPI-06-0505 (2006).

10 Camolotto, S. A. *et al.* FoxA1 and FoxA2 drive gastric differentiation and suppress squamous identity in NKX2-1-negative lung cancer. *Elife* **7**, doi:10.7554/eLife.38579 (2018).

11 Li, C. M. *et al.* Foxa2 and Cdx2 cooperate with Nkx2-1 to inhibit lung adenocarcinoma metastasis. *Genes Dev* **29**, 1850-1862, doi:10.1101/gad.267393.115 (2015).

12 Snyder, E. L. *et al.* Nkx2-1 represses a latent gastric differentiation program in lung adenocarcinoma. *Molecular cell* **50**, 185-199, doi:10.1016/j.molcel.2013.02.018 (2013).

13 Watanabe, H. *et al.* Integrated cistromic and expression analysis of amplified NKX2-1 in lung adenocarcinoma identifies LMO3 as a functional transcriptional target. *Genes Dev* **27**, 197-210, doi:10.1101/gad.203208.112 (2013).

14 Winslow, M. M. *et al.* Suppression of lung adenocarcinoma progression by Nkx2-1. *Nature* **473**, 101-104, doi:10.1038/nature09881 (2011).

15 Bohinski, R. J., Di Lauro, R. & Whitsett, J. A. The lung-specific surfactant protein B gene promoter is a target for thyroid transcription factor 1 and hepatocyte nuclear factor 3, indicating common factors for organ-specific gene expression along the foregut axis. *Mol Cell Biol* **14**, 5671-5681 (1994).

16 Liu, C., Glasser, S. W., Wan, H. & Whitsett, J. A. GATA-6 and thyroid transcription factor-1 directly interact and regulate surfactant protein-C gene expression. *J Biol Chem* **277**, 4519-4525, doi:10.1074/jbc.M107585200 (2002).

17 Yi, M., Tong, G. X., Murry, B. & Mendelson, C. R. Role of CBP/p300 and SRC-1 in transcriptional regulation of the pulmonary surfactant protein-A (SP-A) gene by thyroid transcription factor-1 (TTF-1). *J Biol Chem* **277**, 2997-3005, doi:10.1074/jbc.M109793200 (2002).

18 Bingle, C. D. Thyroid transcription factor-1. *Int J Biochem Cell Biol* **29**, 1471-1473 (1997).

19 Li, Q. *et al.* Stage-dependent and locus-specific role of histone demethylase Jumonji D3 (JMJD3) in the embryonic stages of lung development. *PLoS Genet* **10**, e1004524, doi:10.1371/journal.pgen.1004524 (2014).

20 Lin, S., Perl, A. K. & Shannon, J. M. Erm/thyroid transcription factor 1 interactions modulate surfactant protein C transcription. *J Biol Chem* **281**, 16716-16726, doi:10.1074/jbc.M602221200 (2006).

21 Maeda, Y. *et al.* PARP-2 interacts with TTF-1 and regulates expression of surfactant protein-B. *J Biol Chem* **281**, 9600-9606, doi:10.1074/jbc.M510435200 (2006).

22 Naltner, A., Ghaffari, M., Whitsett, J. A. & Yan, C. Retinoic acid stimulation of the human surfactant protein B promoter is thyroid transcription factor 1 site-dependent. *J Biol Chem* **275**, 56-62 (2000).

23 Park, K. S. *et al.* TAZ interacts with TTF-1 and regulates expression of surfactant protein-C. *J Biol Chem* **279**, 17384-17390, doi:10.1074/jbc.M312569200 (2004).

24 Yang, H., Lu, M. M., Zhang, L., Whitsett, J. A. & Morrisey, E. E. GATA6 regulates differentiation of distal lung epithelium. *Development* **129**, 2233-2246 (2002).

25 Yang, M. C., Guo, Y., Liu, C. C., Weissler, J. C. & Yang, Y. S. The TTF-1/TAP26 complex differentially modulates surfactant protein-B (SP-B) and -C (SP-C) promoters in lung cells. *Biochem Biophys Res Commun* **344**, 484-490, doi:10.1016/j.bbrc.2006.03.158 (2006).

26 Minoo, P. *et al.* Physical and functional interactions between homeodomain NKX2.1 and winged helix/forkhead FOXA1 in lung epithelial cells. *Mol Cell Biol* **27**, 2155-2165, doi:10.1128/MCB.01133-06 (2007).

27 Kaestner, K. H. The FoxA factors in organogenesis and differentiation. *Curr Opin Genet Dev* **20**, 527-532, doi:10.1016/j.gde.2010.06.005 (2010).

28 Bochkis, I. M. *et al.* Genome-wide location analysis reveals distinct transcriptional circuitry by paralogous regulators Foxa1 and Foxa2. *PLoS Genet* **8**, e1002770, doi:10.1371/journal.pgen.1002770 (2012).

29 Kaestner, K. H. The making of the liver: developmental competence in foregut endoderm and induction of the hepatogenic program. *Cell Cycle* **4**, 1146-1148, doi:10.4161/cc.4.9.2033 (2005).

30 Lee, C. S., Friedman, J. R., Fulmer, J. T. & Kaestner, K. H. The initiation of liver development is dependent on Foxa transcription factors. *Nature* **435**, 944-947, doi:10.1038/nature03649 (2005).

31 Gao, N. *et al.* Dynamic regulation of Pdx1 enhancers by Foxa1 and Foxa2 is essential for pancreas development. *Genes Dev* **22**, 3435-3448, doi:10.1101/gad.1752608 (2008).

32 Wan, H. *et al.* Compensatory roles of Foxa1 and Foxa2 during lung morphogenesis. *J Biol Chem* **280**, 13809-13816, doi:10.1074/jbc.M414122200 (2005).

33 Monaghan, A. P., Kaestner, K. H., Grau, E. & Schütz, G. Postimplantation expression patterns indicate a role for the mouse forkhead/HNF-3 alpha, beta and gamma genes in determination of the definitive endoderm, chordamesoderm and neuroectoderm. *Development* **119**, 567-578 (1993).

34 Desai, T. J., Malpel, S., Flentke, G. R., Smith, S. M. & Cardoso, W. V. Retinoic acid selectively regulates Fgf10 expression and maintains cell identity in the prospective lung field of the developing foregut. *Dev Biol* **273**, 402-415, doi:10.1016/j.ydbio.2004.04.039 (2004).

35 Besnard, V., Wert, S. E., Hull, W. M. & Whitsett, J. A. Immunohistochemical localization of Foxa1 and Foxa2 in mouse embryos and adult tissues. *Gene Expr Patterns* **5**, 193-208, doi:10.1016/j.modgep.2004.08.006 (2004).

36 Paranjapye, A., Mutolo, M. J., Ebron, J. S., Leir, S. H. & Harris, A. The FOXA1 transcriptional network coordinates key functions of primary human airway epithelial cells. *Am J Physiol Lung Cell Mol Physiol* **319**, L126-l136, doi:10.1152/ajplung.00023.2020 (2020).

37 Gao, B., Xie, W., Wu, X., Wang, L. & Guo, J. Functionally analyzing the important roles of hepatocyte nuclear factor 3 (FoxA) in tumorigenesis. *Biochim Biophys Acta Rev Cancer* **1873**, 188365, doi:10.1016/j.bbcan.2020.188365 (2020).

38 Bernardo, G. M. & Keri, R. A. FOXA1: a transcription factor with parallel functions in development and cancer. *Biosci Rep* **32**, 113-130, doi:10.1042/BSR20110046 (2012).

39 Robinson, J. L., Holmes, K. A. & Carroll, J. S. FOXA1 mutations in hormone-dependent cancers. *Front Oncol* **3**, 20, doi:10.3389/fonc.2013.00020 (2013).

40 Teng, M., Zhou, S., Cai, C., Lupien, M. & He, H. H. Pioneer of prostate cancer: past, present and the future of FOXA1. *Protein & Cell* **12**, 29-38, doi:10.1007/s13238-020-00786-8 (2021).

41 Cha, Y. J. & Shim, H. S. Biology of invasive mucinous adenocarcinoma of the lung. *Transl Lung Cancer Res* **6**, 508-512, doi:10.21037/tlcr.2017.06.10 (2017).

42 Boggaram, V. Thyroid transcription factor-1 (TTF-1/Nkx2.1/TITF1) gene regulation in the lung. *Clin Sci (Lond)* **116**, 27-35, doi:10.1042/CS20080068 (2009).

43 Hight, S. K. *et al.* An in vivo functional genomics screen of nuclear receptors and their co-regulators identifies FOXA1 as an essential gene in lung tumorigenesis. *Neoplasia* **22**, 294-310, doi:10.1016/j.neo.2020.04.005 (2020).

44 Bejarano, P. A. *et al.* Surfactant proteins and thyroid transcription factor-1 in pulmonary and breast carcinomas. *Mod Pathol* **9**, 445-452 (1996).

45 Young, N. P., Crowley, D. & Jacks, T. Uncoupling cancer mutations reveals critical timing of p53 loss in sarcomagenesis. *Cancer Res* **71**, 4040-4047, doi:10.1158/0008-5472.CAN-10-4563 (2011).

46 Lee, C. L. *et al.* Generation of primary tumors with Flp recombinase in FRT-flanked p53 mice. *Dis Model Mech* **5**, 397-402, doi:10.1242/dmm.009084 (2012).

47 Schonhuber, N. *et al.* A next-generation dual-recombinase system for time- and host-specific targeting of pancreatic cancer. *Nat Med* **20**, 1340-1347, doi:10.1038/nm.3646 (2014).

48 Sund, N. J. *et al.* Hepatocyte nuclear factor 3beta (Foxa2) is dispensable for maintaining the differentiated state of the adult hepatocyte. *Mol Cell Biol* **20**, 5175-5183 (2000).

49 Caswell, D. R. *et al.* Obligate Progression Precedes Lung Adenocarcinoma Dissemination. *Cancer Discovery* **4**, 781-789, doi:10.1158/2159-8290.cd-13-0862 (2014).

50 Marjanovic, N. D. *et al.* Emergence of a High-Plasticity Cell State during Lung Cancer Evolution. *Cancer Cell* **38**, 229-246 e213, doi:10.1016/j.ccell.2020.06.012 (2020).

51 Zou, Z. *et al.* A Single-Cell Transcriptomic Atlas of Human Skin Aging. *Dev Cell* **56**, 383-397.e388, doi:10.1016/j.devcel.2020.11.002 (2021).

52 Song, Y., Washington, M. K. & Crawford, H. C. Loss of FOXA1/2 is essential for the epithelial-to-mesenchymal transition in pancreatic cancer. *Cancer Res* **70**, 2115-2125, doi:10.1158/0008-5472.Can-09-2979 (2010).

53 Little, D. R. *et al.* Transcriptional control of lung alveolar type 1 cell development and maintenance by NK homeobox 2-1. *Proc Natl Acad Sci U S A* **116**, 20545-20555, doi:10.1073/pnas.1906663116 (2019).

54 Little, D. R. *et al.* Differential chromatin binding of the lung lineage transcription factor NKX2-1 resolves opposing murine alveolar cell fates in vivo. *Nat Commun* **12**, 2509, doi:10.1038/s41467-021-22817-6 (2021).

55 Samarasinghe, K. T. G. & Crews, C. M. Targeted protein degradation: a promise for undruggable proteins. *Cell Chem Biol*, doi:10.1016/j.chembiol.2021.04.011 (2021).

56 Miyoshi, H. & Stappenbeck, T. S. In vitro expansion and genetic modification of gastrointestinal stem cells in spheroid culture. *Nature Protocols* **8**, 2471-2482, doi:10.1038/nprot.2013.153 (2013).

57 Han, X. *et al.* Transdifferentiation of lung adenocarcinoma in mice with Lkb1 deficiency to squamous cell carcinoma. *Nat Commun* **5**, 3261, doi:10.1038/ncomms4261 (2014).

58 Dobin, A. *et al.* STAR: ultrafast universal RNA-seq aligner. *Bioinformatics* **29**, 15-21, doi:10.1093/bioinformatics/bts635 (2013).

59 Bushnell, B. *BBtools*, 2021.

60 Liao, Y., Smyth, G. K. & Shi, W. The R package Rsubread is easier, faster, cheaper and better for alignment and quantification of RNA sequencing reads. *Nucleic Acids Research* **47**, e47-e47, doi:10.1093/nar/gkz114 (2019).

61 Love, M. I., Huber, W. & Anders, S. Moderated estimation of fold change and dispersion for RNA-seq data with DESeq2. *Genome Biol* **15**, 550, doi:10.1186/s13059-014-0550-8 (2014).